Research on Single-Hole Compensated Passive Magnetic Shielding Structure for Electric Vehicle Wireless Power Transfer Systems

Zhongqi Li[1,2], Ziyue Gan[1], Liquan Ren[1], Bin Li[1], Pengsheng Kong[3], Hui Li[1], and Junjun Li[3,*]

[1]*College of Electrical and Information Engineering, Hunan University of Technology, Zhuzhou 412007, China*
[2]*College of Electrical and Information Engineering, Hunan University, Changsha 412008, China*
[3]*College of Railway Transportation, Hunan University of Technology, Zhuzhou 412007, China*

ABSTRACT: In the wireless power transfer (WPT) system of electric vehicles, reducing magnetic leakage and minimizing the use of magnetic shielding materials while maintaining transmission efficiency are difficult problems. To this end, a single-hole compensated passive magnetic shielding structure is proposed in this paper, with the system's magnetic leakage reduced and transmission efficiency improved through metal shielding and passive shielding. First, the magnetic shielding principles and design concepts of the magnetic core, aluminum plate, and passive shielding coils are analyzed. The single-hole compensated passive magnetic shielding structure is proposed, and then a mathematical model of the structure is derived. Second, an optimization method is proposed, using Matlab and Ansys Maxwell software to reduce the volume of metallic materials while keeping magnetic leakage within a safe range. Finally, a WPT device based on the proposed structure is constructed according to the optimized magnetic shielding and coil parameters, and the effectiveness of the structure is validated through simulation and experimentation. The results demonstrate that when the system output power is 4 kW, leakage is reduced by 62.7% compared to the single-hole unshielded coil structure using the same materials with the proposed structure. Compared to the all-aluminum plate and all-magnetic core structure, not only is leakage reduced by 1.2%, but there is also a reduction of 40.4% in magnetic core usage and 30.1% in aluminum plate usage. Moreover, the transmission efficiency reaches 93.49%.

1. INTRODUCTION

In recent years, magnetically coupled resonant wireless power transfer (WPT) technology has received extensive attention from scholars and industries [1–3]. WPT systems are characterized by high safety, convenient charging, and resistance to wear and tear. The development of this technology has overcome the limitations of traditional wired power transmission and has been extensively applied in various fields such as implantable medical devices [4], rail transportation [5], and electric vehicles [6]. However, in practical applications, strong magnetic leakage is generated during power transmission. Prolonged exposure to high levels of magnetic leakage can pose certain health risks to humans and also affect the normal operation of electronic devices. Therefore, to balance the efficiency of the WPT system and reduce magnetic leakage, metal materials such as magnetic cores [7] and aluminum plates, along with shielding coils, are often placed near the coils. It is essential to minimize the amount of metal while maintaining high transmission efficiency to ensure magnetic leakage safety, thereby reducing system costs. This approach represents one of the crucial directions for the development of wireless power transfer technology.

At present, scholars have conducted research in the field of magnetic shielding and have proposed various shielding methods, including active shielding, passive shielding, and metal shielding [8, 9].

Active shielding reduces magnetic leakage in WPT systems by generating a counteracting magnetic field opposite to the leakage field using a shielding coil with an external excitation source [10]. Cruciani et al, proposed an active shielding method, which involves placing the shielding coil in series with the transmitting coil on the same horizontal plane [11]. This method achieves the suppression of magnetic fields in specific spatial regions, while reducing 50% of the magnetic field, and still maintains high efficiency. However, it only serves to reduce the leakage in local areas and requires larger coil sizes. Two shielding coils were placed at the transmitting end of the WPT system by the Campi's team [12], while ensuring transmission, the magnetic field in specific areas near the WPT coil is reduced, but no experimental validation has been conducted.

The shielding coil in passive shielding generates a counteracting magnetic field in the opposite direction of the magnetic field of the main coil through electromagnetic induction without requiring external excitation [13]. Adjusting the size of the matching capacitance to change the magnetic field direction of the shielding coil is utilized to minimize magnetic leakage around the system by forming an angle between the shielding coil magnetic field direction and the main coil magnetic field direction. This method addresses the issue of magnetic field

* Corresponding author: Junjun Li (862739748@qq.com).

weakening caused by a fixed current and offers high flexibility. Kim et al. have proposed a reactive resonance shielding method that relies on tuned capacitance [14]. This method achieves the optimal capacitor combination by obtaining the magnetic induction intensity of test points, reducing the magnetic field by 64%. However, the specific impact of this shielding method on the system's transmission efficiency is not specified.

Metal shielding involves adding metallic materials such as magnetic cores and aluminum plates to the WPT system to minimize magnetic leakage in the surrounding area. Metallic materials need to be carefully designed due to their high cost and large size. Chen and Cheng confirmed that the core material possesses characteristics that enhance transmission efficiency and reduce magnetic leakage [15]. After the insertion of the magnetic core into the WPT system, an increase in power transmission efficiency of approximately 30% is observed within the transmission distance range of 60 mm to 80 mm. However, higher costs are incurred due to the use of a single whole magnetic core. The structural shape of the core is also a factor that affects its shielding performance. While using a whole core is effective, it also comes with the disadvantages of high consumables and costs. Therefore, Kim et al. [16] compared the performance of U-type and E-type cores and concluded that U-type cores offer better shielding performance, but their material design leads to increased costs and system size. Budhia et al. [17] studied the shielding performance of type I cores on double D coils. Type I cores can significantly reduce the material volume and cost of cores, but they have low system transmission efficiency.

Zhu et al. researched the shielding of aluminum plates [18]. A magnetic shielding scheme placing the aluminum plate on one side of the vehicle was investigated. However, the shielding effect of this scheme is limited and does not consider the impact of different shielding methods on the system's transmission efficiency. Afterwards, Wang et al. used double-layer aluminum plates to enhance the shielding [19]. Compared to a single-layer aluminum plate shielding structure, the magnetic field was reduced by 89.5% with the double-layer aluminum plate composite shielding structure, but this led to further increased material consumption. In addition, Rong et al. analyzed the magnetic shielding effect of a grid aluminum plate [20], although it reduces the use of materials, it only addresses the local area of magnetic leakage, which has limitations. To enhance the shielding effect, metal shielding is often combined with passive shielding and active shielding to provide magnetic shielding for the WPT system. Mi et al. proposed a double-ring active shielding coil directly connected in series with the transmitting coil, which eliminates the additional coupling between the shielding coil and the receiving coil [21], but the structure uses a whole core and aluminum plate, which increases costs, and in the event of coil deflection, transmission efficiency is reduced. Ref. [22] discusses the use of a complete core with an active shielding coil for combined shielding. This approach reduces system leakage and enhances system transmission efficiency, but the cost of using a complete core is substantial. The utilization of magnetic core materials was optimized by Gu et al. [23], with the magnetic core combined in blocks with soft magnetic composite materials, which reduced the utiliza-

tion rate of the magnetic core by 63% and decreased the leakage magnetic field by 8%. However, the manufacturing process is complex, and maintenance costs are higher. Qin et al. utilized a multilayer core combined with an aluminum plate to minimize magnetic leakage [24] and used polytetrafluoroethylene (PTFE) material to optimize system transmission efficiency and reduce core loss, but the structure requires more materials and is more complex. In the wireless charging system for electric vehicles, reducing magnetic leakage in the system through magnetic shielding technology while saving materials has become an urgent issue.

A single-hole compensated passive magnetic shielding structure is proposed, and joint dynamic optimization of the magnetic core, aluminum plate, and shielding coil is conducted. The optimization results indicate that when the system output power is 4 kW, leakage is reduced by 62.7% compared to the single-hole unshielded coil structure using the same materials with the proposed structure. Compared to the all-aluminum plate and all-magnetic core structure, not only is leakage reduced by 1.2%, but there is also a reduction of 40.4% in magnetic core usage and 30.1% in aluminum plate usage. This leads to a significant reduction in production costs and system volume. Moreover, the transmission efficiency decreases by only about 4% when the system has a maximum offset of 10 cm. Furthermore, an experimental platform was constructed to validate the reliability of this structure.

2. CALCULATION OF MAGNETIC FIELD STRENGTH

In this section, a method for calculating the magnetic induction strength of a rectangular coil is provided [25], which offers a theoretical basis for determining the dimensions of the transmitter and receiver coils that follow.

Figure 1 shows the spatial distribution of two rectangular coils $Coil_1$ and $Coil_2$. a_1 and a_2 are the length and width of $Coil_1$, and b_1 and b_2 are the length and width of $Coil_2$. $Coil_1$ is divided into four parts (l_1, l_2, l_3, l_4), and parameter I denotes the current flowing through $Coil_1$.
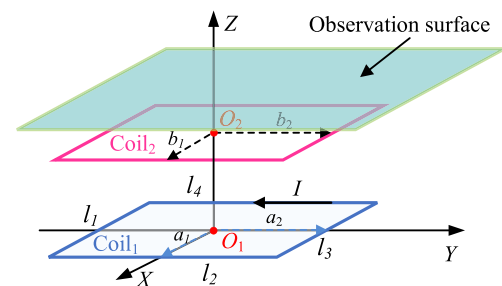

FIGURE 1. Schematic diagram of spatial distribution of rectangular coil.

An arbitrary point $P(x, y, z)$ in the space is set in Figure 1, and the expression for the vector magnetic potential is as follows:

$$A(x, y, z) = \frac{\mu_0}{4\pi} \int_v \frac{J(x', y', z') \, dv'}{R} \tag{1}$$

where J is the current density; v is the current distribution in the conductor; and R is the distance from any point P to the point source (x', y', z').

The magnetic induction B is related to the vector magnetic potential by the following equation:

$$B = \nabla \times A \tag{2}$$

After double Fourier transform operations and circuit analysis, the magnetic induction intensity components on the X-axis, Y-axis, and Z-axis can be obtained as follows:

$$B_x(x, y, z) = \frac{1}{4\pi^2} \int_{-\infty}^{\infty} \int_{-\infty}^{\infty} C_{ix} \cdot e^{-kz} \cdot e^{j(x\xi+y\eta)} d\xi d\eta \tag{3}$$

$$B_y(x, y, z) = \frac{1}{4\pi^2} \int_{-\infty}^{\infty} \int_{-\infty}^{\infty} C_{iy} \cdot e^{-kz} \cdot e^{j(x\xi+y\eta)} d\xi d\eta \tag{4}$$

$$B_z(x, y, z) = \frac{1}{4\pi^2} \int_{-\infty}^{\infty} \int_{-\infty}^{\infty} C_{iz} \cdot e^{-kz} \cdot e^{j(x\xi+y\eta)} d\xi d\eta \tag{5}$$

$$C_{ix} = \frac{-j2\mu_0 I \sin(\xi a_1) \sin(\eta a_2)}{\eta} \cdot e^{s_1 k} \tag{6}$$

$$C_{iy} = \frac{-j2\mu_0 I \sin(\xi a_1) \sin(\eta a_2)}{\xi} \cdot e^{s_1 k} \tag{7}$$

$$C_{iz} = \frac{-2\mu_0 I k \sin(\xi a_1) \sin(\eta a_2)}{\xi \eta} \cdot e^{s_1 k} \tag{8}$$

where ξ and η are the double Fourier integral variables

$$k = \sqrt{\xi^2 + \eta^2} \tag{9}$$

therefore, the magnetic induction can be expressed as:

$$B = \sqrt{|B_x|^2 + |B_y|^2 + |B_z|^2} \tag{10}$$

In the application of static wireless charging for electric vehicles, it is essential to consider the impact of magnetic leakage around the system on both human bodies and equipment. Therefore, this paper conducts a magnetic shielding observation based on the actual scenario. The observation is the magnetic leakage observation surface at a distance of 10 cm from the top of the WPT system, as illustrated in Figure 1.

3. SINGLE-HOLE COMPENSATED PASSIVE MAGNETIC SHIELD STRUCTURE

In order to minimize magnetic leakage within the interior space of electric vehicles during charging, a single-hole compensated passive magnetic shielding coil structure is proposed. In this structure, metal materials are perforated, and passive shielding coils are added to reduce magnetic leakage on the observation surface.

In this section, the magnetic shielding principles of magnetic cores, aluminum plates, and passive shielding coil structures are first analyzed. Subsequently, a single-hole compensated passive magnetic shielding coil structure is proposed. This structure is found to have a good magnetic shielding effect from both physical and mathematical perspectives, and it significantly reduces the amount of metal material required and lowers fabrication costs.

3.1. Single-Hole Compensated Passive Magnetic Shield Structure and Principle Analysis

The single-hole compensated passive magnetic shielding structure utilizes a magnetic core, an aluminum plate, and a passive shielding coil for combined shielding. The magnetic shielding effect of this structure after perforating the core and the aluminum plate is investigated. It aims to reduce the system volume and production cost by minimizing the use of metal materials, and passive shielding coils are added to compensate the increase in magnetic leakage caused by reducing the metal material.

3.1.1. Core Shield Structure Analysis

The core material has the characteristics of high permeability and low magnetic loss. Therefore, the magnetic field between the transmission coils can be concentrated by incorporating a magnetic core into the WPT system. By adding a magnetic core, the leakage of the magnetic field can be limited; interference with the surrounding environment and other equipment can be reduced; and electromagnetic shielding can be served. Additionally, the magnetic field can be concentrated, and the magnetic induction strength can be enhanced by the magnetic core. Therefore, the magnetic core can improve the magnetic coupling between the transmission coils, helping to reduce energy loss in the energy transmission process and enhance the transmission efficiency of the WPT system.

Since the core material is characterized by its large size and high cost, this paper focuses on designing and optimizing the core shape. To conserve materials, this paper utilizes a single-hole core structure. The core volume V_T and mutual inductance M for various core structures are illustrated in Figure 2. The magnetic field distribution diagram demonstrates the magnetic shielding effect of different core types.

According to Figure 2, the core exhibits good magnetic field constraint ability, reducing magnetic leakage around the WPT system. Moreover, the use of more core materials increases the mutual inductance value, resulting in higher transmission efficiency. Type 2 incorporates a whole core on the outside of the WPT system, which effectively concentrates the magnetic field and significantly reduces the magnetic field surrounding the system. However, this design requires more core material. Therefore, Type 3 incorporates a single-hole core on the outside the WPT system, covering the coil. From the magnetic field distribution diagram, it can be observed that by reducing the core material, the magnetic field constraint ability is weakened, and the mutual inductance M is greatly reduced, which leads to lower system transmission efficiency than Type 2. In order to reduce the amount of magnetic core material while maintaining high transmission efficiency, Type 4 is based on the Type 3 structure with an inner edge formed by raising the inner circle of the magnetic core. The structures of the transmitting end and receiving end are identical. The details of the Type 4 magnetic core are shown in Figure 3. As shown in Figure 2. its magnetic inductance confinement capability is comparable to that of Type 3, but Type 4 has a higher mutual inductance value and only a small increase in core usage. Therefore, the core structure of Type 4 is utilized in this paper. In order to reduce
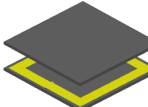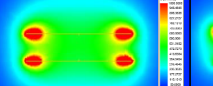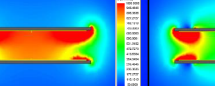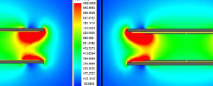
	Type Ⅰ：coil	Type Ⅱ：Full coverage magnetic core	Type Ⅲ：Single- hole magnetic core	Type Ⅳ: Single-hole magnetic core With inner edge
Simulation model				
Magnetic field distribution				
M and magnetic core V_T	M=63.44µH	M=149.46µH V_T=5400cm^3	M=111.46µH V_T=3000cm^3	M=126.74µH V_T=3164cm^3

FIGURE 2. Comparison of magnetic field diagrams, mutual inductance values, and core volumes for different types of cores.
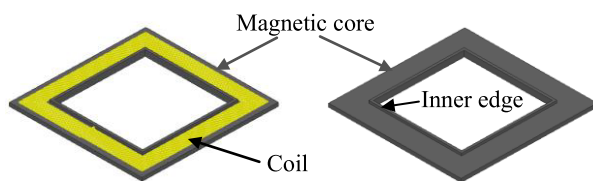

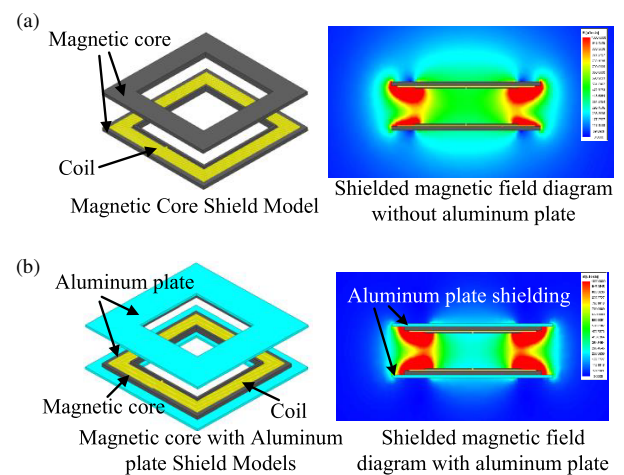
FIGURE 3. Magnetic core structure.

FIGURE 4. Aluminum plate core shielding effect comparison. (a) Aluminum-free plate shielding model and magnetic field diagram. (b) Aluminum plate shielding model and magnetic field diagram available.

the magnetic leakage from the observation surface of the WPT system to a safe value or less, it is also necessary to include an aluminum plate with a shielding coil in the structure and to optimize the core structure dimensions.

3.1.2. Aluminum Plate Shielding Structure Analysis

As a conductive material, aluminum plates can absorb and reflect electromagnetic waves, thus preventing the propagation of leaked magnetic flux lines and reduces external environmental interference on the system, thereby increasing the stability and reliability of the WPT system. When magnetic flux lines pass through aluminum plates, eddy currents are induced on the surface of the aluminum plates. Energy is consumed by these eddy currents and converted into heat. The thermal losses caused by the eddy current effect in the metal shield are reduced by the magnetic core. Therefore, the combination of aluminum plates and magnetic cores results in a good magnetic shielding effect.

The magnetic core can suppress magnetic leakage above the receiving end to a certain extent. However, to further reduce magnetic leakage, adding an aluminum plate above the magnetic core significantly decreases the magnetic leakage above the system, as shown in Figure 4. This reduction occurs because the eddy current is mainly concentrated in the aluminum plate, effectively cancels out the magnetic field.

As shown in Figure 4, an aluminum plate is added to the magnetic shielding below the transmitting end and above the receiving end of the WPT system, and the aluminum plate absorbs the surrounding magnetic leakage, significantly reducing magnetic leakage at the target observation surface, resulting in a highly effective magnetic shielding effect. The eddy current field distribution of the aluminum plate is shown in Figure 5.
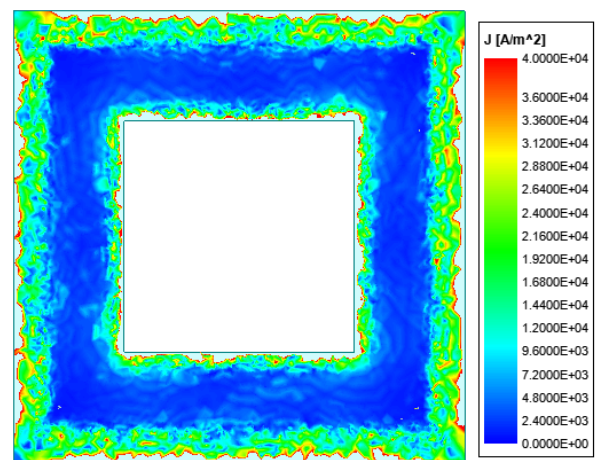

FIGURE 5. Aluminum plate vortex field diagram.

3.1.3. Passive Shielded Coil Principle Analysis

The single-hole compensated passive magnetic shielding structure reduces the use of magnetic core and aluminum plate ma-
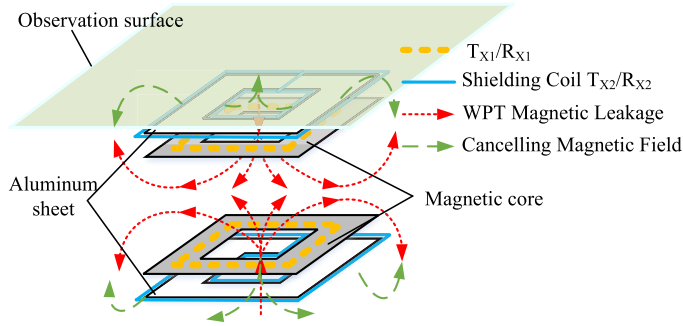
FIGURE 6. Schematic diagram of passive shielding coil magnetic shielding principle.

FIGURE 7. Schematic superposition of coil magnetic field vectors.

terials, and the shielding effect is weakened. In order to keep the magnetic leakage at the observation surface at a safe value of 27 μT or less, it is necessary to add a passive shielding coil to the structure to reduce the magnetic leakage at the observation surface.

The principle of the passive shielding coil of the system is shown in Figure 6. The anti-series zigzag passive shielding coil is positioned parallel to the aluminum plate. When the shielding coil receives the magnetic field from the transmitting and receiving coils, an induced voltage V_{ind} is generated across the shielding coil with the following expression:

$$V_{\text{ind}} = \int E \cdot dl = -\frac{d\phi}{dt} = -\frac{dB \cdot S}{dt} \quad (11)$$

where B is the time-varying leakage magnetic field generated by the transmitting and receiving coils, whose expression can be expressed as:

$$B = B_0 e^{j\omega t} = B_0 \cos \omega t + jB_0 \sin \omega t \quad (12)$$

substituting (12) into (11) gives the induced voltage expression as:

$$V_{\text{ind}} = -j\omega B_0 e^{j\omega t} S \quad (13)$$

the shielding coil impedance can be expressed as $Z_{sh} = R_{sh} + j\omega L_{sh} - 1/j\omega C_{sh}$, and the coil internal resistance R_{sh} is negligible. Then, the current I_{sh} in the shielded coil can be expressed as:

$$I_{\text{sh}} = \frac{-j\omega B_0 e^{j\omega t} S}{j\omega L_{\text{sh}} - \frac{1}{\omega C_{\text{sh}}}} \quad (14)$$

according to Biosavar's law, the offset magnetic field generated by the shielded coil can be expressed as:

$$B_{\text{sh}} = -B \cdot \frac{\mu_0 j\omega S}{4\pi j \left(\omega L_{\text{sh}} - \frac{1}{\omega C_{\text{sh}}}\right)} \int_{c'} \frac{\overrightarrow{dl} \times \overrightarrow{R}}{R^3} \quad (15)$$

It is easy to see that when $\omega L_{sh} > 1/\omega C_{sh}$, the B_{sh} and B are reversed, and the coil can have a shielding effect of magnetic leakage.
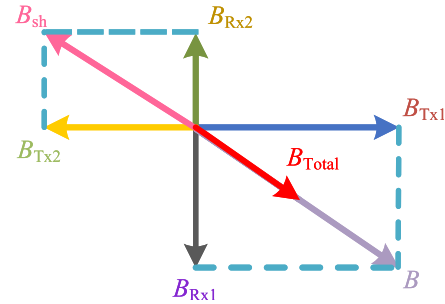
In order to illustrate the principle of coil magnetic field weakening more intuitively, the coil magnetic field vector superposition schematic is introduced, as shown in Figure 7. The magnetic field vector of the transmitting coil T_{X1} is B_{TX1}, and the magnetic field vector of the receiving coil R_{X1} is denoted as B_{RX1}. The matching capacitance of the passive shielding coil is adjusted so that the direction of the magnetic field of the shielding coils T_{X2} and R_{X2} is opposite to the direction of the magnetic field of the main coils to achieve the effect of reducing the leakage of magnetism, and thus the magnetic field B_{sh} synthesized by the shielding coils is in the opposite direction of the synthesized field B of the main coils, which reduces the leakage of magnetism from the observation surface.

3.2. Structure and Mathematical Modeling of Single-Hole Compensated Passive Magnetic Shielding

The single-hole compensated passive magnetic shielding structure proposed in this paper uses an aluminum plate, a magnetic core, and a shielding coil to shield the magnetic leakage from the observation surface. Because the metal material has the disadvantage of large volume and high cost, this paper digs holes in the metal material, and the single-hole compensated passive magnetic shielding structure after reducing the metal material is shown in Figure 8.

The schematic diagram of the single-hole compensated passive magnetic shielding structure is depicted in Figure 8(a). This structure is composed of transmitting coil T_{X1}, receiving coil R_{X1}, shielding coils T_{X2} and R_{X2}, as well as a magnetic core and an aluminum plate. The transmitting coil T_{X1} is positioned above the magnetic core, while the shielding coil T_{X2} is placed parallel to the aluminum plate below the magnetic core. The receiving end structure is symmetrically distributed at a distance of 15 cm above the transmitting end. The receiving coil R_{X1} is situated below the magnetic core, and the shielding coil R_{X2} is placed parallel to the aluminum plate above the magnetic core. A top view of the transmitting end of this structure is provided by Figure 8(b), which illustrates the composition of the single-hole compensated passive magnetic shielding structure in a more intuitive manner.

In order to reduce the metal material of the WPT system and thus reduce the cost, the aluminum plate and magnetic core ma-
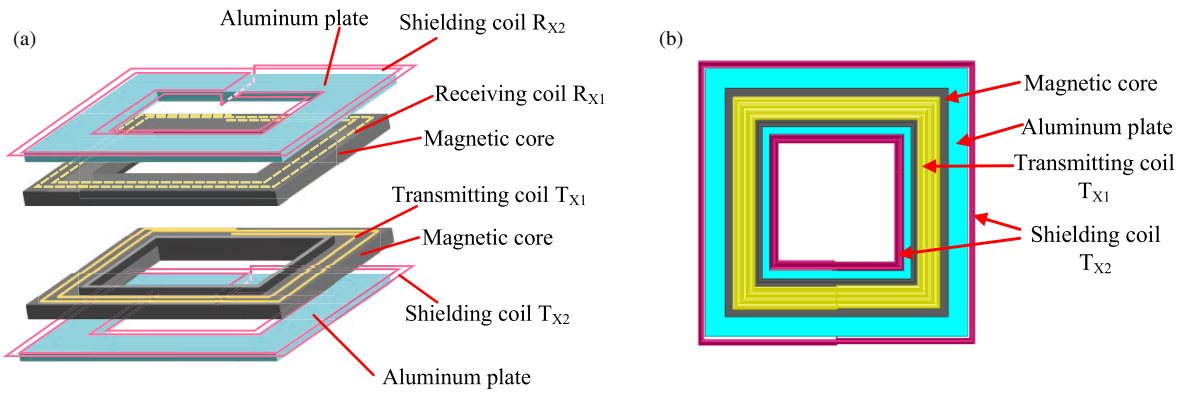
FIGURE 8. Spatial structure of single-hole compensated passive magnetic shielding structure. (a) Schematic diagram of single-hole compensated passive magnetic shield structure. (b) Top view of transmitting end of single-aperture compensated passive magnetic shielding structure.
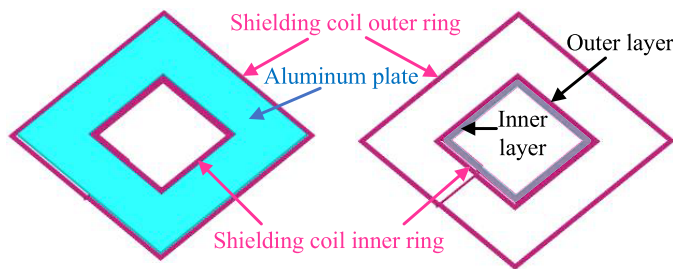

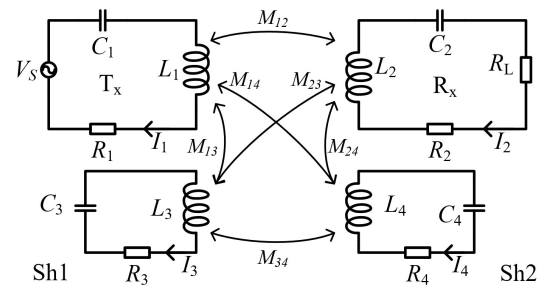**FIGURE 9**. Passive shielded coil structure.

FIGURE 10. Passive shielded coil structure.

terials are dug out, and the inner edge is added to the inner ring of the core to increase the coupling between the main coils, and the core structure is shown in Figure 3. However, reducing the materials of the aluminum plate and core can result in an increase in magnetic leakage at the observation surface. To mitigate this, a passive shielding coil is incorporated into the WPT system to minimize magnetic leakage at the observation surface. The shielding coil is parallel to the aluminum plate as shown in Figure 9. Meanwhile, in order to counteract the impact of the passive shielding coil on the efficiency of the WPT system, the shielding coil in the inner ring of the aluminum plate is divided into two layers. The inner layer is used to minimize

magnetic leakage, and the outer layer is used to reduce the influence on the efficiency of the main coil. The structure of the passive shielding coil is shown in Figure 9.

According to the structure diagram of single-hole compensated passive magnetic shield in Figure 7, the corresponding equivalent circuit diagram of the system is obtained as shown in Figure 10.

L_i and R_i are the self-inductance and internal resistance of each coil ($i = \{1, 2, 3, 4\}$); C_1 is the resonant capacitance of the transmitting coil; C_2 is the resonant capacitance of the receiving coil; C_3 and C_4 are the matching capacitance of the shielding coil, which is used to control the shielding current phase and current amplitude; M_{ij} is the mutual inductance between coils i and j ($i, j = \{1, 2, 3, 4\}$); V_S is the transmitting coil excitation; R_L is the load.

A matrix of Kirchhoff voltage equations can be derived from the circuit diagram of Figure 10 represented by Eq. (16).

$$\begin{bmatrix} [t]Z_1 & j\omega M_{12} & j\omega M_{13} & j\omega M_{14} \\ j\omega M_{21} & Z_2 & j\omega M_{23} & j\omega M_{24} \\ j\omega M_{31} & j\omega M_{32} & Z_3 & j\omega M_{34} \\ j\omega M_{41} & j\omega M_{42} & j\omega M_{43} & Z_4 \end{bmatrix} \begin{bmatrix} I_1 \\ I_2 \\ I_3 \\ I_4 \end{bmatrix} = \begin{bmatrix} V_S \\ 0 \\ 0 \\ 0 \end{bmatrix} \quad (16)$$

From the above matrix, the currents of each coil are obtained as shown in Eq. (17), where impedance $Z_1 = R_1$, $Z_2 = R_2 + R_L$, $Z_3 = R_3 + j\omega L_3 - 1/j\omega C_3$, $Z_4 = R_4 + j\omega L_4 - 1/j\omega C_4$. The transmission efficiency η can be obtained from Eq. (17) as shown in Eq. (18):
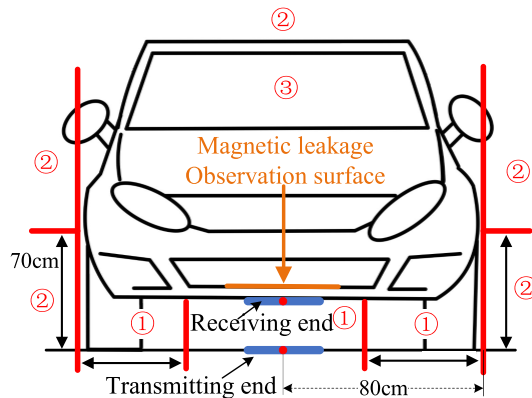

FIGURE 11. Schematic diagram of leakage magnetic field target surface.

$$I_1 = \frac{V_s \left[\omega^2 Z_4 (M_{14}^2 + M_{24}^2) + Z_2 Z_4^2\right]}{\omega^2 \left[M_{14}^2 (\omega^2 M_{14}^2 - 2\omega^2 M_{24}^2 + Z_2 Z_4) + M_{24}^2 (\omega^2 M_{24}^2 + Z_2 Z_4) + M_{12} Z_4 (M_{12} Z_4 - 4j\omega M_{14} M_{24})\right]}$$

$$I_2 = \frac{-2V_s Z_4 (jM_{12} + \omega M_{14} M_{24})}{\omega \left[M_{14}^2 (\omega^2 M_{14}^2 - 2\omega^2 M_{24}^2 + Z_2 Z_4) + M_{24}^2 (\omega^2 M_{24}^2 + Z_2 Z_4) + M_{12} Z_4 (M_{12} Z_4 - 4j\omega M_{14} M_{24})\right]}$$

$$I_3 = \frac{-V_s \left[j\omega^2 M_{24} (M_{24}^2 - M_{14}^2) + Z_4 (\omega M_{12} M_{14} + j\omega M_{24} Z_2)\right]}{\omega \left[M_{14}^2 (\omega^2 M_{14}^2 - 2\omega^2 M_{24}^2 + Z_2 Z_4) + M_{24}^2 (\omega^2 M_{24}^2 + Z_2 Z_4) + M_{12} Z_4 (M_{12} Z_4 - 4j\omega M_{14} M_{24})\right]}$$

$$I_4 = \frac{-V_s \left[jM_{14} (\omega^2 M_{14}^2 - \omega^2 M_{24}^2 + Z_2 Z_4) + \omega M_{12} M_{24} Z_4\right]}{\omega \left[M_{14}^2 (\omega^2 M_{14}^2 - 2\omega^2 M_{24}^2 + Z_2 Z_4) + M_{24}^2 (\omega^2 M_{24}^2 + Z_2 Z_4) + M_{12} Z_4 (M_{12} Z_4 - 4j\omega M_{14} M_{24})\right]}$$

$$(17)$$

$$\eta = \frac{(M_{12} Z_4 - 2j\omega M_{14} M_{24})^2}{M_{14}^2 (\omega^2 M_{14}^2 - 2\omega^2 M_{24}^2 + Z_2 Z_4) + M_{24}^2 (\omega^2 M_{24}^2 + Z_2 Z_4) + M_{12} Z_4 (M_{12} Z_4 - 4j\omega M_{14} M_{24})}$$
$$\cdot \frac{-Z_4 R_L}{V_S \left[\omega^2 (M_{14}^2 + M_{24}^2) + Z_2 Z_4\right]}$$

$$(18)$$

4. LEAKAGE OPTIMIZATION

In order to prevent the magnetic leakage generated by the WPT system from harming the human body, a single-hole compensated passive magnetic shielding structure is proposed to solve the problem of magnetic field leakage inside the car. According to the standard SAEJ2954 safety specification for electromagnetic fields in electric vehicles, the magnetic shielding protection area is divided into three areas as shown in Figure 11, in which areas 2 and 3 are the human activity areas, and the magnetic leakage should be within the safety range value of 27 µT. When the system is installed with a metal shield, the magnetic leakage in region 2 is small and generally meets the safety standard value. Therefore, it is necessary to shield the magnetic leakage in region 3 (inside the car) so that it remains within the safety limit of 27 µT. The observation surface for magnetic leakage is located in the upper 10 cm of the receiving coil.

In this section, the dimensions of the transmitting coil T_{X1} and receiving coil R_{X1} are firstly determined according to the magnetic induction strength calculation formula (10). Subsequently, the overall parameters of the single-aperture compensated passive magnetic shielding structure are optimized using Ansys Maxwell software. The specific optimization process includes adjusting the dimensional parameters of the aluminum plate, magnetic core, and passive shielding coil structure, aiming to ensure that the maximum magnetic leakage on the observation surface is less than 27 µT, while minimizing the use of aluminum plate and magnetic core.

The flow of optimization is shown in Figure 12, and the specific optimization steps are as follows:

(1) Parameter setting and initialization: The vertical transmission distance between the transmitting and receiving coils is set to 15 cm. The length and width of the inner edges of the transmitting and receiving coils are both 40 cm; the numbers of turns are both 15; and the parameter sizes are in line with the dimensions of the chassis of the vehicle in which they are installed. The passive shielding coil is at the same level as the aluminum plate. The conductor is made of copper wire, with a cross-section diameter of 0.4 cm. The magnetic shield is assembled using a core with dimensions of $10 * 10 * 1.5$ cm; the inner edge of the core is assembled using a core with dimensions of $1.5 * 7.5 * 1$ cm; and the transmission power is set at 4 kW.

(2) Setting constraints: The optimization objective is to reduce the magnetic leakage from the observation surface and at the same time reduce the amount of material, so the core and aluminum plate size should be as close as possible to the size of the transmitting and receiving coils, and set according to the actual situation: the length of the aluminum plate and the outer edge of the core is set at 65–75 cm, and the length of the inner edge is set at 30–40 cm. The number of turns for the inner layer of the shielding coil's inner ring is set to 5–8, and the number of turns for the outer layer of the shielding coil's inner ring is set to 2–5, and the number of turns of the outer ring of the shielding coils is set to 2–5. When the step size is selected, the smaller the step size is, the more detailed the data obtained will be, but the amount of data will also increase, leading to longer computation times. Therefore, an appropriate step size should be chosen based on the requirements. In this study, the step size for the number of turns is set to 1 turn, and the step size for the side length is set to 1 cm.

(3) System simulation to obtain the leakage B and transmission efficiency η: The observation surface leakage and the system transmission efficiency are obtained based on the simulation results, and the maximum leakage is recorded for this system parameter.

(4) Condition judgment: The optimization requirements are assessed for the current system parameters B and η. If the maximum magnetic leakage on the observation surface is less than the safe leakage value of 27 µT and the transmission efficiency equal to or greater than 96%, the optimization criteria are met. The current parameters are saved, and adjustments are made to continue optimization. If the optimization criteria are not met, the current parameters are not saved, and adjustments are made directly to continue optimization.
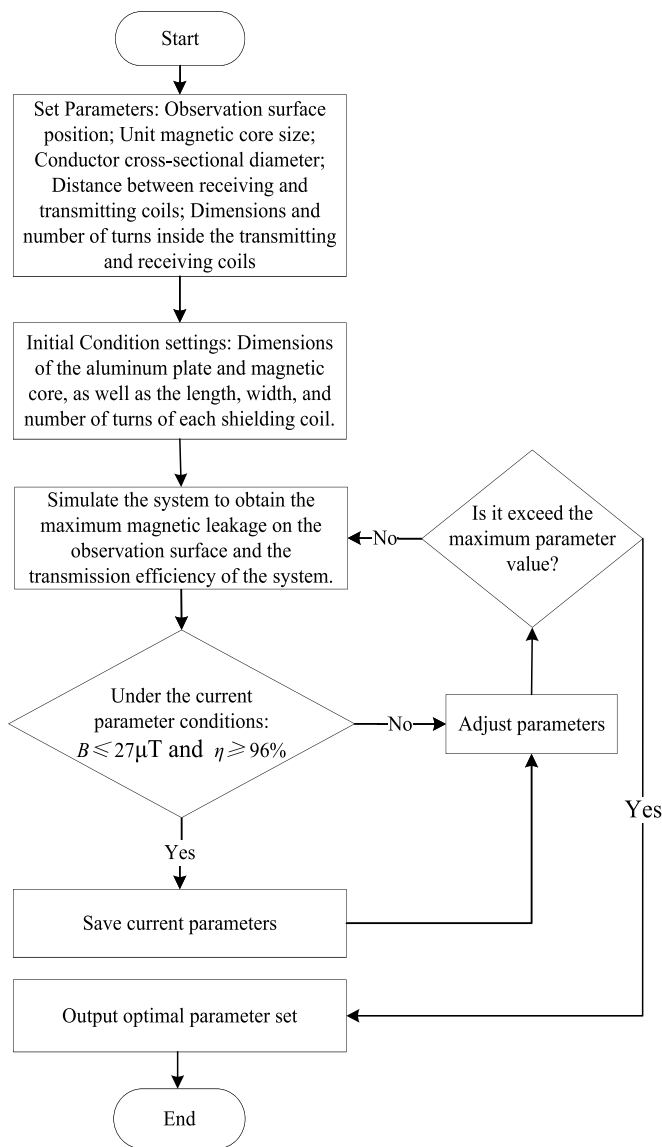
FIGURE 12. Coil structure optimization process.

5. EXPERIMENTAL VERIFICATION

In this section, the single-hole compensated passive magnetic shielding structure is simulated and experimentally verified. The Ansys Maxwell software and Matlab software are used to get the simulated values of the maximum leakage value B and transmission efficiency η at the observation surface of the system, and a set of 4 kW experimental platforms is built. The experimental results show that there is a small error between the simulated and the experimental values of the maximum magnetic leakage and transmission efficiency at the observation surface, which validates the accuracy of the structure. The effectiveness of the structure is proved by comparing the maximum leakage value B and transmission efficiency η of three different shielding structures.

5.1. Detailed Parameters of the Experimental Device

The experimental system framework is shown in Figure 13. Initially, DC power is inverted into AC power by the inverter module. Subsequently, energy is transmitted from the transmitting coil to the receiving coil in the WPT module. Finally, AC power is converted into DC power for load usage by the rectifier module. Both the inverter and rectifier modules are single-phase full-bridge circuits, capable of handling a maximum current of 30 A.

The main components of the experimental test platform are composed of a load, a WT5000 power analyzer, an RT-unit inverter-rectifier module, an oscilloscope, a physical coil model, a DC power supply, and an NF-5035S electromagnetic radiation analyzer, as shown in Figure 14(a). A physical coil model was constructed based on the parameters obtained from the optimization process, with all coils wound using Litz wire. The Litz wire specifications are $\phi 0.1\,\text{mm} \times 800$ strands, capable of handling a maximum current of 31.4 A. The physical model includes a transmitting coil, a receiving coil, two shield coils, two combined magnetic cores, and two aluminum plates, as illustrated in Figure 14(b). Additionally, the WT5000 power analyzer is utilized to test the system's transmission ef-

(5) Adjust parameters: Based on the preset constraints, the size range and step sizes are adjusted. Each time one variable is changed, the maximum magnetic leakage on the observation surface and the system transmission efficiency are obtained. Then, according to the optimization requirements, size parameters are continuously adjusted until all parameters within the constraints are cycled through, and the optimal set of parameters is outputted.

(6) Output the optimal matrix parameters: The system parameters with the observation surface below 27 μT safe leakage are output. The final system parameters are as follows: the outer edge of the core is 60 cm, and the inner edge is 40 cm; the outer edge of the aluminum plate is 71 cm, and the inner edge is 36 cm; the number of turns for the inner layer of the inner ring of the shielding coil is 6, and the length of the outer edge is 36 cm; the number of turnsfor the outer layer of the inner ring of the shielding coil 4, and the length of the inner edge is 36 cm; the number of turns in the outer ring of the shielding coil is 4, and the length of the inner edge is 71 cm.

TABLE 1. Physical parameters of the coil.

|		
$L_1/\mu\text{H}$	Self-inductance of transmitting coil	355
$L_2/\mu\text{H}$	Self-inductance of receiving coil	353
$L_3/\mu\text{H}$	Self-inductance of lower shielding coil	38
$L_4/\mu\text{H}$	Self-inductance of upper shielding coil	37
C_1/nF	Resonant capacitance of transmitting coil	10
C_2/nF	Resonant capacitance of receiving coil	9
C_3/nF	Lower shielded coil matching capacitance	119
C_4/nF	Upper shielded coil matching capacitance	119
$R_1/\text{m}\Omega$	Parasitic resistance of transmitting coil	427
$R_2/\text{m}\Omega$	Parasitic resistance of receiving coil	409
$R_3/\text{m}\Omega$	Parasitic resistance of lower shielding coil	218
$R_4/\text{m}\Omega$	Upper shielded parasitic resistance	226
f_0/kHz	Operating frequency	85
R_L/Ω	Load	30
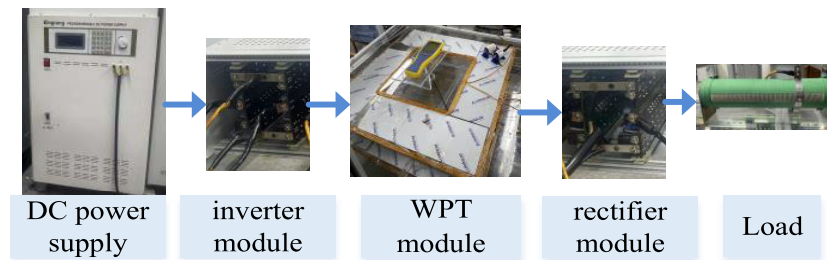
FIGURE 13. System frame diagram.
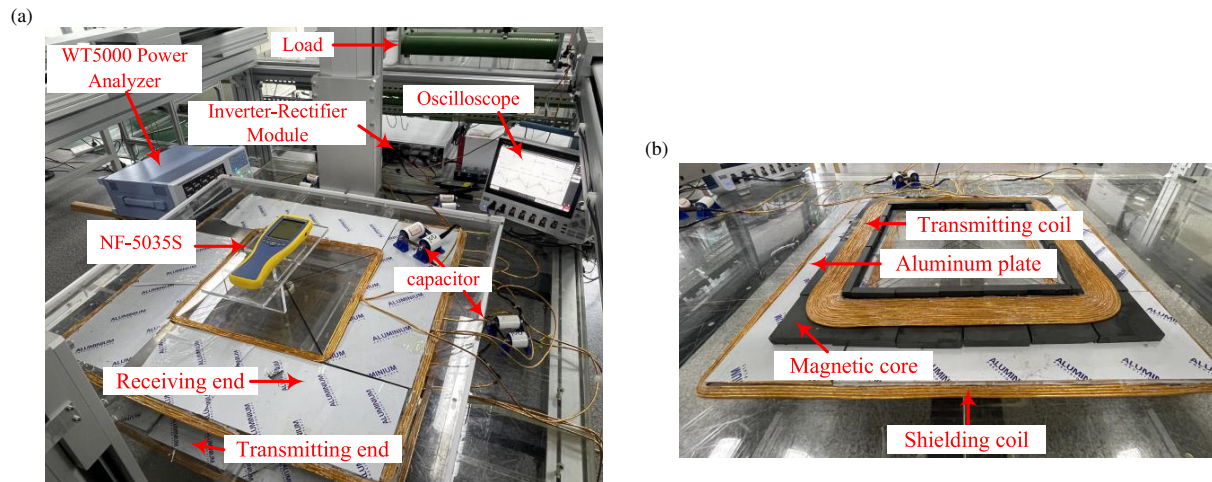
FIGURE 14. Overall experimental map. (a) Experimental platforms. (b) Single-hole compensated passive magnetic shield structure physical detail drawing.

ficiency; the NF-5035S electromagnetic radiation analyzer is used to observe magnetic leakage on the observation surface; and the IM3536 impedance analyzer is employed to measure the detailed physical parameters of this structure as shown in Table 1.

5.2. Magnetic Leakage of the System

In order to test the magnetic leakage of the system, this subsection compares the magnetic leakage of the WPT all-aluminum-plate full-core shielded system, the WPT single-hole unshielded coil system, and the WPT single-hole compensated coil shielded system. Initially, three different coil models of the structures are drawn using Ansys Maxwell software. Then, the coil models are simulated to obtain the magnetic field distribution and the maximum simulated magnetic leakage value B_s at the observation surface. Finally, the maximum magnetic leakage experimental value B_e at the observation surface is obtained using the electromagnetic radiation analyzer NF-5035S.

5.2.1. WPT All-Aluminum Plate Full-Core Shielding System

Figure 15(a) depicts the schematic diagram of the WPT all-aluminum plate full-core shielding system. The square aluminum plate has a side length of 732 mm and a thickness of

10 mm. The square magnetic core has a side length of 600 mm and a thickness of 15 mm.

Figure 15(b) shows the magnetic leakage distribution on the observation surface of the all-aluminum plate full-core shielding system at a maximum offset of 10 cm, with a maximum magnetic leakage of 26.6 μT.

Figure 15(c) illustrates the variation in maximum magnetic leakage at different distances of receiver offset. It can be observed that the maximum magnetic leakage on the observation surface increases with the increase in offset distance. Due to the effective magnetic shielding effect of the aluminum plate and core, the experimentally measured maximum magnetic leakage at a 10 cm offset is 25.7 μT, which is below the safety standard of 27 μT. However, this structure has the drawback of being bulky and costly in practical applications, so the structure of this paper improves the all-aluminum plate full-core shielding system.

5.2.2. WPT Single Hole Unshielded Coil System

5.2.3. Single-Hole Compensated Passive Magnetic Shielding System

Figure 16(a) shows a schematic diagram of the WPT single hole unshielded coil system. In this case, the square aluminum plate has an outer edge length of 710 mm, an inner edge length of 360 mm, and a thickness of 10 mm. The square magnetic core
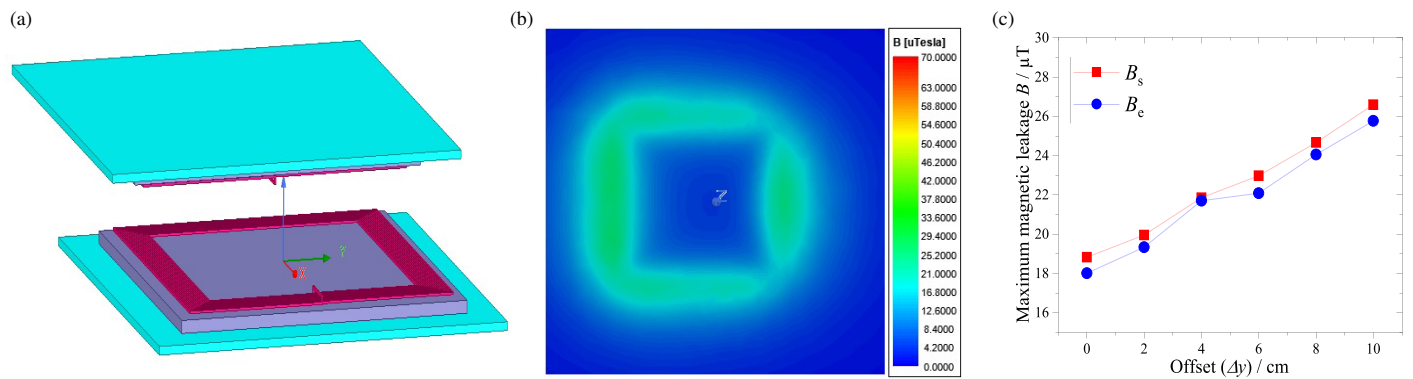
FIGURE 15. WPT all-aluminum plate full-core shielding system. (a) Schematic diagram of WPT's all-aluminum, all-core shielding system. (b) Target surface leakage distribution of WPT's all-aluminum, all-core shielding system. (c) All-aluminum plate full-core shielding system leakage at offset.
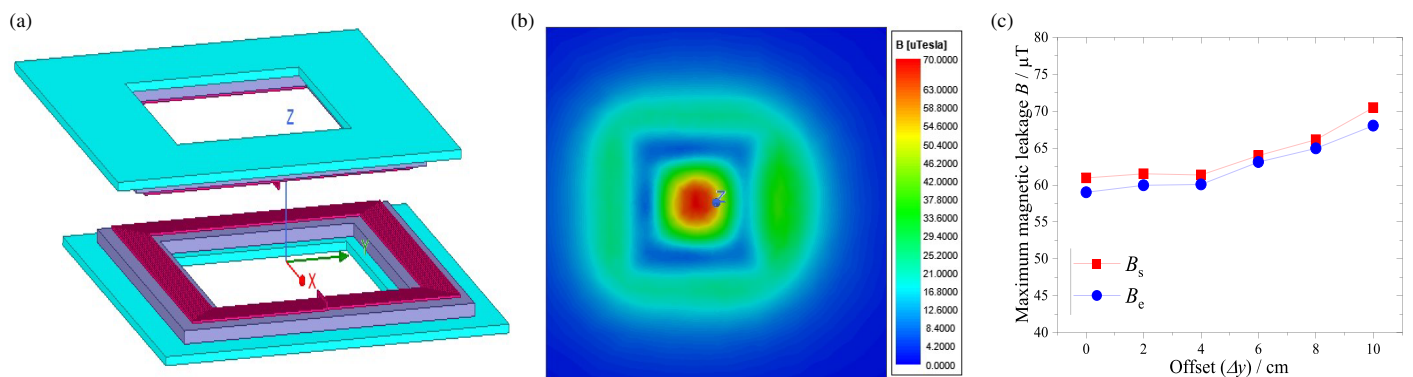

FIGURE 16. WPT single hole unshielded coil system. (a) Schematic diagram of WPT single hole unshielded coil system. (b) Target surface leakage distribution of WPT single hole unshielded coil system. (c) Single hole unshielded coil system leakage at offset.

has an outer edge length of 600 mm, an inner edge length of 400 mm, and a thickness of 15 mm.

Figure 16(b) shows the distribution of magnetic leakage on the observation surface for this system at a maximum offset of 10 cm, with a maximum leakage of 70 μT on the observation surface.

Figure 16(c) shows the variation of maximum magnetic leakage under different offsets. At an offset of 10 cm, the experimentally measured maximum magnetic leakage is 68.1 μT. A single-hole magnetic core aluminum plate structure is proposed to reduce the volume and cost of the WPT system. However, it can be seen from Figure 16(b) that saving magnetic core and aluminum plate materials will result in increased magnetic leakage at the observation surface. Therefore, based on the magnetic leakage distribution diagram shown in Figure 16(b), shielding coils are added to the WPT system to reduce magnetic leakage at the observation surface.

Figure 17(a) shows a schematic diagram of the WPT single-hole compensated passive magnetic shielding system. The square aluminum plate has an outer edge length of 710 mm, an inner edge length of 360 mm, and a thickness of 10 mm, and the square magnetic core has an outer edge length of 600 mm, an inner edge length of 400 mm, and a thickness of 15 mm.

Figure 17(b) shows the distribution of magnetic leakage on the observation surface when the maximum offset of the system is 10 cm, and the maximum magnetic leakage on the observation surface is 26.3 μT. Comparing Figure 17(b) with Figure 16(b), it can be seen that the addition of shielding coils to the WPT system significantly reduces the leakage of magnetic leakage on the observation surface and has a good magnetic shielding effect.

Figure 17(c) shows the variation of the maximum leakage at different offset distances, with the experimentally measured maximum leakage of 25.4 μT at an offset of 10 cm.

It can be concluded that the single-hole compensated passive magnetic shielding system, compared to the WPT all-aluminum plate full-core shielding system, reduces approximately 30.1% of aluminum plate material and 40.4% of core material while maintaining nearly identical magnetic leakage at the observation surface. Compared to the single-hole unshielded coil system, under the same aluminum plate and core conditions, the maximum magnetic leakage is reduced by approximately 63.4%. Therefore, the single-aperture compensated passive magnetic shielding structure still has good magnetic shielding capability while saving material.
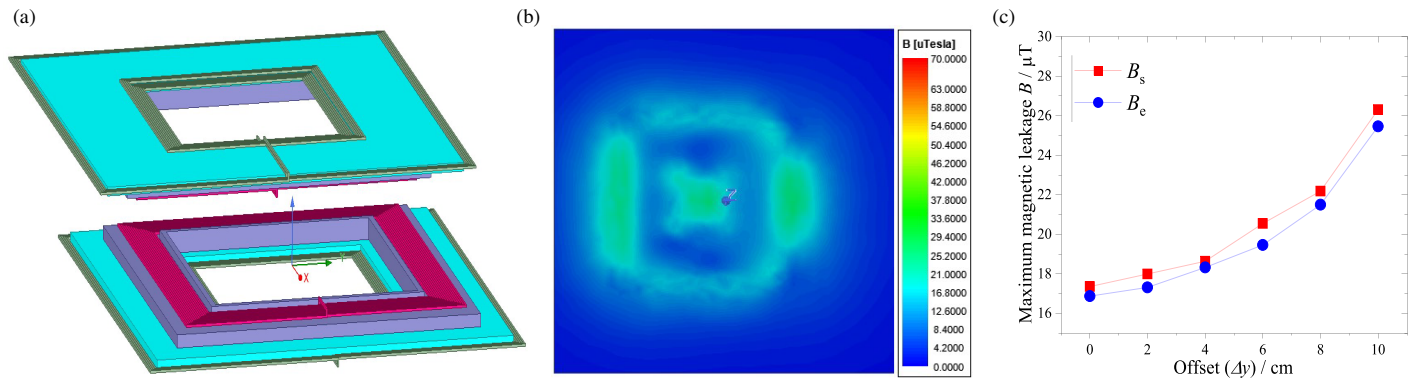
FIGURE 17. WPT single hole unshielded coil system. (a) WPT single hole compensated passive magnetic shielding system. (b) Target surface leakage distribution of single hole compensated passive magnetic shielding system. (c) Single-hole compensated passive magnetic shielding system leakage at offset.
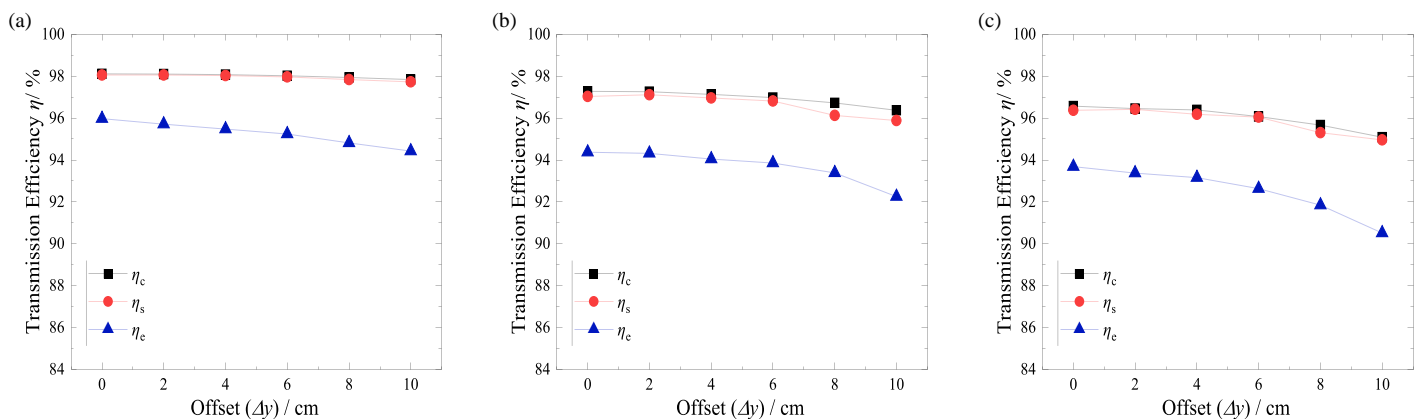

FIGURE 18. Transmission efficiency under different shielding conditions. (a) Transmission efficiency of an all-aluminum, all-core shielding system. (b) Transmission efficiency of single-hole unshielded coil systems. (c) Single-hole compensated passive magnetic shielding system transmission efficiency.

5.3. System Transmission Efficiency

In order to measure the variation of system transmission efficiency with different offset distances, simulation parameters for the core, aluminum plate, and coils are first obtained using Ansys Maxwell software. These simulation parameters are then utilized in the transmission efficiency expression (18) to derive the theoretical value of system transmission efficiency η_c. Subsequently, the simulation value of system transmission efficiency, η_s, is obtained using Matlab/Simulink software. Finally, the experimental value of system transmission efficiency, η_e, is measured using the WT5000 power analyzer. By comparing the transmission efficiencies of the three different structures at the same offset distance, further analysis of the single-hole compensated passive magnetic shielding structure was conducted.

Figure 18 shows the system efficiency under different off-set conditions. Certain differences between the simulated and experimental results are observed. This is due to the use of metallic materials in some experimental equipment and slight deviations between the experimental model and simulation model during fabrication. Therefore, measurement errors occur during the experimental measurements, leading to discrepancies

between the simulated and experimental results. However, the experimental error is within 5%.

The data in Figure 18 indicate that as the offset distance increases, the system efficiency gradually decreases, reaching its lowest value at a 10 cm offset. Furthermore, by comparing the three different shielding structures, it can be observed that the single-hole compensated passive magnetic shielding structure proposed in this study reduces a significant amount of magnetic leakage and materials compared to the WPT all aluminum plate full-core shielding structure, with only approximately a 4% decrease in transmission efficiency. Additionally, it reduces approximately 30.1% of aluminum plate material and 40.4% of core material.

Comparisons of the proposed structure with other WPT systems are provided, including shielding methods, material savings rates, magnetic leakage, and transmission efficiency after shielding, as shown in Table 2, where B_z represents the magnetic leakage on the horizontal observation surface above the receiving, and B_{xy} represents the magnetic leakage on the vertical observation surface 80 cm away from the center of the vehicle chassis. It can be concluded that compared to other systems, the single-hole compensated passive magnetic shielding

TABLE 2. Comparison of different existing magnetic shielding solutions.

Literatures	Shielding method	Material savings	$B_z/\mu T$	$B_{xy}/\mu T$	Efficiency
[22]	Fe+Passive coil	No savings	more than 27	\	90.30%
[24]	Fe+Al	No savings	\	\	92.30%
[26]	Fe	81.24% Magnetic core	more than 27	\	71.52%
[27]	Fe	85.00%Magnetic core	73	\	91.00%
[28]	Fe+Al+Cu	No savings	\	24.8	92.10%
[29]	Fe+Al	No savings	\	14.4	91.20%
This paper	Fe+Al+Passive coil	40.40% Magnetic core 30.10% Aluminum plate	16.87	1.26	93.49%

structure proposed in this study maintains high transmission efficiency while reducing material usage, and it achieves the lowest magnetic leakage in WPT systems.

6. CONCLUSION

A single-hole compensated passive magnetic shielding structure is proposed in this paper. The main features of this structure include magnetic core and aluminum plate hole-digging, which reduce the metal materials. Additionally, passive shielding coils are utilized to further decrease magnetic leakage from the observation surface, while enhancing the transmission efficiency of the system. With the WPT single-hole compensated passive magnetic shielding structure, the maximum magnetic leakage on the observation surface can be kept below $27\,\mu T$ at $4\,kW$ output power with a $\pm 10\,cm$ Y-axis offset. This design saves approximately 30.1% of the aluminum plate material and 40.4% of the magnetic core material compared to the all-aluminum plate and all-magnetic core shielding structure. It also reduces magnetic leakage by about 63.4% compared to the single-hole unshielded coil structure using the same material.

This structure can effectively reduce magnetic leakage at the observation surface within a safe range while minimizing the use of magnetic core and aluminum plate materials, demonstrating practical value. It can be applied in the wireless charging field of electric vehicles. In the future, further research can be conducted on porous magnetic cores and aluminum plates to further reduce material costs while ensuring shielding effectiveness and achieving higher transmission efficiency.

ACKNOWLEDGEMENT

REFERENCES

[1] Zhang, X., L. Ren, P. Kong, X. Xiong, and Z. Li, "Study of a double-layer passive magnetic shielding system for electric vehicle WPT," *Progress In Electromagnetics Research C*, Vol. 137, 65–79, 2023.

[2] Li, Z. Q., X. B. Xiong, P. S. Kong, and L. Q. Ren, "Research on electromagnetic shielding and efficiency optimization technology of wireless power transfer system," *Journal of Electronic Measurement and Instrumentation*, Vol. 37, No. 5, 151–162, 2023.

[3] Cheng, J. Y., X. L. Wu, and Z. F. Bai, "Maximum efficiency tracking of wireless power transfer for electric vehicles based on coupling coefficient estimation," *Journal of Electronic Measurement and Instrumentation*, Vol. 34, No. 3, 180–186, 2020.

[4] Chen, W., Z. Liu, Z. Li, X. Yan, and K. Qian, "Research on multi coil reactive shielding of resonant wireless energy supply cardiac pacemaker," *Transaction of China Electrotechnical Society*, Vol. 37, No. 11, 2673–2685, 2022.

[5] Chen, K., Y. Jiang, T. Tan, *et al.*, "Research on 350 kW high power wireless power transfer system for rail transit," *Transactions of China Electrotechnical Society*, Vol. 37, No. 10, 2411–2421, 2022.

[6] Wang, Z., X. Wang, B. Zhang, *et al.*, "Advances of wireless charging technology in electric vehicle," *Journal of Power Supply*, Vol. 12, No. 3, 27–32, 2014.

[7] Zhang, X., P. Zhang, Q. Yang, Z. Yuan, and H. Su, "Magnetic shielding design and analysis for wireless charging coupler of electric vehicles based on finite element method," *Transactions of China Electrotechnical Society*, Vol. 31, No. 1, 71–79, 2016.

[8] Dou, R. T., *et al.*, "Review on the application development and research of electromagnetic shielding of magnetically coupled resonant wireless power transfer system," *Proceedings of the CSEE*, Vol. 43, 6020–6040, 2023.

[9] Li, J. Y., H. Wen, K. Zhang, *et al.*, "Research progress on electromagnetic interference suppression of magnetically coupled wireless power transfer system," *Proceedings of the CSEE*, Vol. 42, 7387–7403, 2022.

[10] Meng, J., Y. Zhang, Y. J. Guo, *et al.*, "Research of active magnetic shielding for wireless power transfer system of electric vehicles," *Advanced Technology of Electrical Engineering and Energy*, Vol. 40, No. 4, 44–51, 2021.

[11] Cruciani, S., T. Campi, F. Maradei, and M. Feliziani, "Active shielding design for a dynamic wireless power transfer system," in *2020 International Symposium on Electromagnetic Compatibility — EMC Europe*, 1–4, Rome, Italy, 2020.

[12] Campi, T., S. Cruciani, F. Maradei, and M. Feliziani, "Active coil system for magnetic field reduction in an automotive wireless power transfer system," in *2019 IEEE International Symposium on Electromagnetic Compatibility, Signal & Power Integrity (EMC+SIPI)*, 189–192, New Orleans, LA, USA, 2019.

[13] Kim, S., H.-H. Park, J. Kim, J. Kim, and S. Ahn, "Design and analysis of a resonant reactive shield for a wireless power electric vehicle," *IEEE Transactions on Microwave Theory and Techniques*, Vol. 62, No. 4, 1057–1066, 2014.

[14] Kim, J., J. Kim, S. Kong, H. Kim, I.-S. Suh, N. P. Suh, D.-H. Cho, J. Kim, and S. Ahn, "Coil design and shielding methods for a magnetic resonant wireless power transfer system," *Proceedings of the IEEE*, Vol. 101, No. 6, 1332–1342, 2013.

[15] Chen, M. X. and K. W. E. Cheng, "Design of flat magnetic core for inductively coupled coils in high efficiency wireless power transfer application," in *2017 7th International Conference on Power Electronics Systems and Applications — Smart Mobility, Power Transfer & Security (PESA)*, 1–7, Hong Kong, China, 2017.

[16] Kim, C.-G., D.-H. Seo, J.-S. You, J.-H. Park, and B.-H. Cho, "Design of a contactless battery charger for cellular phone," *IEEE Transactions on Industrial Electronics*, Vol. 48, No. 6, 1238–1247, 2001.

[17] Budhia, M., J. T. Boys, G. A. Covic, and C.-Y. Huang, "Development of a single-sided flux magnetic coupler for electric vehicle IPT charging systems," *IEEE Transactions on Industrial Electronics*, Vol. 60, No. 1, 318–328, 2013.

[18] Zhu, Q., D. Chen, L. Wang, C. Liao, and Y. Guo, "Study on the magnetic field and shielding technique for an electric vehicle oriented wireless charging system," *Transactions of China Electrotechnical Society*, Vol. 30, No. S1, 143–147, 2015.

[19] Wang, S., B. Wei, X. Wu, C. Xu, J. Xu, W. Ge, and J. Xu, "Electromagnetic shielding design for magnetic coupler of N-type dynamic electric vehicle wireless power transfer systems," in *2019 22nd International Conference on Electrical Machines and Systems (ICEMS)*, 1–7, Harbin, China, 2019.

[20] Rong, C., X. Tao, C. Lu, and M. Liu, "Investigation of magnetic field shielding by mesh aluminum sheet in wireless power transfer system," in *2019 IEEE Wireless Power Transfer Conference (WPTC)*, 126–129, London, UK, 2019.

[21] Mi, M., Q. Yang, Y. Li, P. Zhang, and W. Zhang, "Multi-objective active shielding coil design for wireless electric vehicle charging system," *IEEE Transactions on Magnetics*, Vol. 58, No. 2, 1–5, 2022.

[22] Dai, Z., X. Zhang, T. Liu, C. Pei, T. Chen, R. Dou, and J. Wang, "Magnetic coupling mechanism with omnidirectional magnetic shielding for wireless power transfer," *IEEE Transactions on Electromagnetic Compatibility*, Vol. 65, No. 5, 1565–1574, 2023.

[23] Gu, B. S., T. Dharmakeerthi, S. Kim, M. J. O'Sullivan, and G. A. Covic, "Optimised magnetic core layer in inductive power transfer pad for electric vehicle charging," *IEEE Transactions on Power Electronics*, Vol. 38, No. 10, 11 964–11 973, 2023.

[24] Qin, R., J. Li, J. Sun, and D. Costinett, "Shielding design for high-frequency wireless power transfer system for EV charging with self-resonant coils," *IEEE Transactions on Power Electronics*, Vol. 38, No. 6, 7900–7909, 2023.

[25] Li, Z. Q., S. Y. Li, J. Li, *et al.*, "Mutual inductance calculation and optimization of multiple receiving coils in positive and negative series structure for dynamic wireless energy transmission system," *Journal of Electrotechnology*, Vol. 36, No. 24, 5153–5164, 2021.

[26] Rituraj, G. and P. Kumar, "A new magnetic structure of unipolar rectangular coils in WPT systems to minimize the ferrite volume while maintaining maximum coupling," *IEEE Transactions on Circuits and Systems II: Express Briefs*, Vol. 68, No. 6, 2072–2076, 2021.

[27] Pearce, M. G. S., G. A. Covic, and J. T. Boys, "Reduced ferrite double D pad for roadway IPT applications," *IEEE Transactions on Power Electronics*, Vol. 36, No. 5, 5055–5068, 2021.

[28] Mohammad, M., E. T. Wodajo, S. Choi, and M. E. Elbuluk, "Modeling and design of passive shield to limit EMF emission and to minimize shield loss in unipolar wireless charging system for EV," *IEEE Transactions on Power Electronics*, Vol. 34, No. 12, 12 235–12 245, 2019.

[29] Pearce, M. G. S., G. A. Covic, and J. T. Boys, "Robust ferrite-less double D topology for roadway IPT applications," *IEEE Transactions on Power Electronics*, Vol. 34, No. 7, 6062–6075, 2019.